# An Anisotropic Plasticity Model for Quasi-Brittle Composite Shells

**P.B. Lourenço**[1]

**Abstract.** A material model for the analysis of anisotropic plates and shells is described. The proposed plasticity model includes two different yield criteria: one to represent tensile failure and another to represent compressive failure. The model describes adequately the failure behaviour of cohesive-frictional materials, with large differences in the magnitude of uniaxial tensile and compressive strength. Additionally, independent elastic and inelastic behaviour can be described along each material axis. To validate the numerical implementation, a comparison between experimental and numerical results in masonry shell panels is also presented.

## 1 INTRODUCTION

It is known that most structural materials exhibit some degree of anisotropy. Materials, such as timber, are naturally anisotropic, cold-worked metal sheets manifest predominant-directional properties which are intensified with increasing degree of plastic deformation. Other materials are anisotropic due to the manufacturing process such as plywood, reinforced concrete, masonry and most laminated composites.

The difficulties in accurately modelling the behaviour of anisotropic materials are, usually, quite strong. This is due, not only, to the fact that comprehensive experimental results (including pre- and post-peak behaviour) are generally lacking, but also to intrinsic difficulties in the formulation of anisotropic inelastic behaviour. To describe the failure behaviour of anisotropic composites a criterion is needed which is able to describe the complex phenomena that govern failure in this type of materials. Criteria such as those of Hill [1], Hoffman [2] and Tsai-Wu [3] have been defined with the aim of meeting this requirement. These anisotropic plasticity models have been proposed both from purely theoretical and experimental standpoints as failure criteria. But only a few numerical implementations and calculations have actually been carried out. Examples are given by the work of de Borst and Feenstra [4] and Schellekens and de Borst [5] which fully treated the implementation, in modern plasticity algorithmic concepts, of, respectively, an elastic-perfectly-plastic Hill yield criterion and an elastic-perfectly-plastic Hoffman yield criterion. In principle, inelastic behaviour could be simulated with the fraction model of Besseling [6] but not much effort has been done in this direction.

In fact, one of the serious problems that remains associated to the application of the above criteria is the description of inelastic behaviour. Besides the fraction model, other attempts can be found in the work of Owen and Figueiras [7], which included material-axis-dependent hardening in the Hill criterion, Swan and Cakmak [8], which included linear tensorial hardening in the Hill yield criterion, and Li *et al* [9], which included linear hardening in a modified (pressure dependent) Von Mises criterion to fit either the uniaxial tensile or compressive behaviour. Nevertheless, all these approaches to model inelastic behaviour are relatively crude. In this article, the approach of [7] is extended to include softening behaviour and independent fracture energies along each material axis.

The other problem associated with criteria such as Hill, Hoffman and Tsai-Wu is the poor representation of materials with a large difference between uniaxial compressive strength and uniaxial tensile strength, Lourenço [10]. Due to the smoothness of these criteria, unacceptable overestimation of strength can be found in the tension-compression regime. Figure 1 illustrates the problem of aiming to represent a plane stress isotropic no-tension material with such anisotropic paraboloid yield criteria.

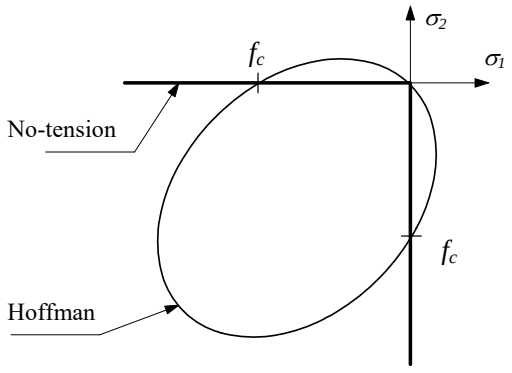


**Figure 1 Plane stress representation of the Hoffman criterion and a no-tension material ($f_c$ is the uniaxial compressive strength)**

To obtain a better representation of materials with considerable difference in the magnitude between compressive and tensile strength, individual yield criteria are considered, according to different failure mechanisms, one in tension and the other in compression. The former is associated with a localised fracture process, denoted by cracking of the material, and, the latter, is associated with a more distributed fracture process which is usually termed crushing of the material. The material model has been

[1] Department of Civil Engineering, University of Minho, Azurém, P-4800 Guimarães, Portugal. Also at the Faculty of Civil Engineering, Delft University of Technology, The Netherlands

developed for shells, which represents an extension of the work previously carried out for plane stress, Lourenço *et al* [11]. It is noted that a representation of an anisotropic yield criterion solely in terms of principal stresses is not possible. For shells, which is the case of the present article, a graphical representation in terms of the full stress vector in a predefined set of material axes is necessary. Anisotropic material behaviour including a Hill type criterion for compression and a Rankine type criterion for tension is proposed. This represents an extension of conventional formulations for isotropic quasi-brittle materials to describe anisotropic behaviour. In particular, it is an extension of the work of Feenstra and de Borst [12], who utilised this approach for concrete with a Rankine and a Drucker-Prager criterion.

Modern algorithmic plasticity concepts - including implicit Euler backward return mapping schemes and consistent tangent operators for all regimes of the model - are utilised to combine anisotropic elastic behaviour with anisotropic plastic behaviour. The proposed yield criterion combines the advantages of modern plasticity concepts with a powerful representation of anisotropic material behaviour, which includes different hardening/softening behaviour along each material axis. It is thus capable of reproducing independent (in the sense of completely diverse) elastic and inelastic behaviour along a prescribed set of material axes. The energy-based regularisation technique, which is employed to obtain objective results with respect to mesh refinement, resorts then to four different fracture energies.

The numerical implementation and performance of the model is evaluated by means of a comparison between numerical results and experimental results for the case of masonry panels with out-of-plane loading.

# 2 DESCRIPTION

## 2.1 Adopted Shell Element

The finite element adopted is the curved shell element degenerated from a 3-D formulation. This element, originally proposed by Ahmad *et al* [13] for the linear analysis of moderately thick shells, has been extensively used for the geometrical and non-linear analysis of shell structures.

Typical characteristics of this element are the two hypotheses on which the degeneration is based: “straight normals” and “zero normal stress”. The first hypothesis assumes that the normals to the mid-plane of the element remain straight after deformation, but not necessarily perpendicular to the mid-plane. The second hypothesis states that the normal stress component perpendicular to the mid-plane equals zero, and the element formulation has been obtained ignoring the strain energy resulting from this stress. Assuming that the local *z*-axis represents the normal to the mid-plane, the five stress components left are $\sigma_x$, $\sigma_y$, $\tau_{xy}$, $\tau_{yz}$ and $\tau_{xz}$.

Five degrees of freedom are defined for each element node: three translations and two rotations, see Figure 2. The definition of the independent translations and rotations includes the influence of shear deformation. The rotations are not coupled to the gradient of the mid-plane.

In this article, two by two Gauss integration in plane and seven-point Simpson integration in the thickness direction are used.

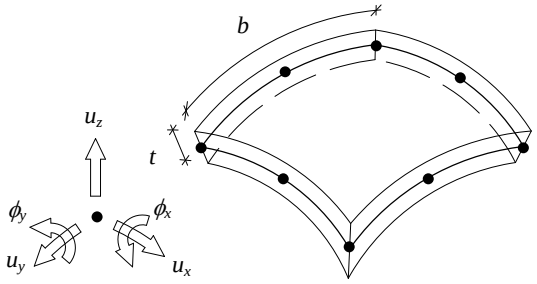


**Figure 2 Curved shell element (applicable for thin shells with t << b)**

## 2.2 Thin Shells and its Plane Stress Behaviour

For laminated structures (plates and shells with one dimension substantially smaller than the other two dimensions), the behaviour is typically two-dimensional, see Figure 3, and it is possible to adopt a yield criterion developed for plane stress conditions enhanced with the two new stress components.

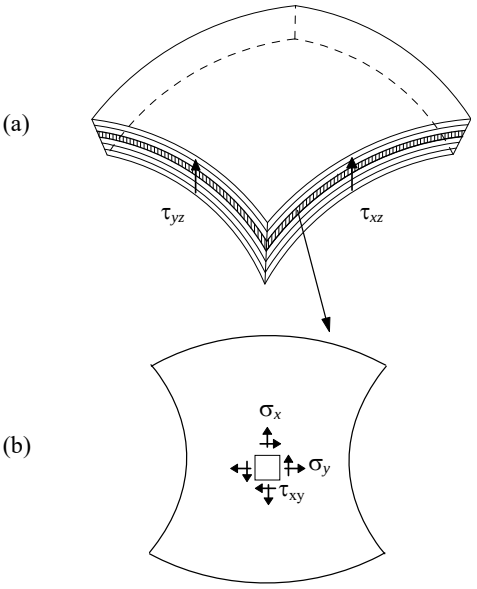


**Figure 3 Thin shells. (a) Layered shell with five stress components; (b) Layer, essentially, in plane stress conditions**

Therefore, the adopted yield criterion is based on the plane stress anisotropic yield criterion of [11] which includes a Hill type criterion for compression and a Rankine type criterion for tension, see Figure 4. Note that the word *type* is used here because the yield criteria adopted are close to the original yield criteria. Nevertheless, they represent solely a fit of experimental results.

The implementation of the model in modern algorithmic plasticity concepts - implicit Euler backward return mapping, local and global Newton-Raphson method, consistent tangent stiffness and proper treatment of the singular points - has been fully described in [11] and will not be reviewed here. In the following, only constitutive aspects, with particular reference to the shell behaviour, will be discussed.

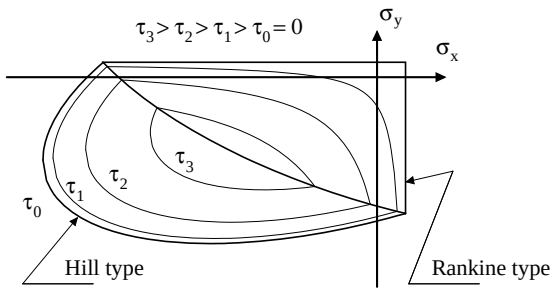


**Figure 4 Proposed plane stress composite yield criterion with iso-shear stress lines**

## 2.3 Tension - A Rankine Type Criterion

For modelling tensile behaviour, it will be assumed that cracks, at each integration point, always arise normal to the mid-surface of the element. This assumption means that each layer of the shell element is considered to be in plane stress and the additional stresses from the shell formulation ($\tau_{yz}$ and $\tau_{xz}$) will be ignored. Of course, the assumption entails some approximation as diagonal "shear" cracks in the thickness direction are replaced by cracks stepwise normal to the mid-surface. Nevertheless, this is a widely used simplification in thin shell analysis which, for the case of anisotropic shells, becomes particularly attractive because the input data are heavily reduced. In particular, the material behaviour along the z-axis (normal to the element mid-plane) and the contribution to failure of the two additional shear stresses do not have to be described.

An adequate formulation of the Rankine criterion is given by a single function, which is governed by the first principal stress and one yield value $\overline{\sigma}_t$ that describes the softening behaviour of the material as, see [14],

$$f_1 = \frac{\sigma_x + \sigma_y}{2} + \sqrt{\left(\frac{\sigma_x - \sigma_y}{2}\right)^2 + \tau_{xy}^2} - \overline{\sigma}_t(\kappa_t) \qquad (1)$$

where the scalar $\kappa_t$ controls the amount of softening. This expression can be rewritten as

$$f_1 = \frac{(\sigma_x - \overline{\sigma}_t(\kappa_t)) + (\sigma_y - \overline{\sigma}_t(\kappa_t))}{2} + \sqrt{\left(\frac{(\sigma_x - \overline{\sigma}_t(\kappa_t)) - (\sigma_y - \overline{\sigma}_t(\kappa_t))}{2}\right)^2 + \tau_{xy}^2} \qquad (2)$$

where coupling exists between the stress components and the yield value. Setting forth a Rankine type criterion for an anisotropic material, with different tensile strengths along the *x*, *y* directions, is now straightforward if eq. (2) is modified to

$$f_1 = \frac{(\sigma_x - \overline{\sigma}_{tx}(\kappa_t)) + (\sigma_y - \overline{\sigma}_{ty}(\kappa_t))}{2} + \sqrt{\left(\frac{(\sigma_x - \overline{\sigma}_{tx}(\kappa_t)) - (\sigma_y - \overline{\sigma}_{ty}(\kappa_t))}{2}\right)^2 + \alpha\tau_{xy}^2} \qquad (3)$$

where the parameter α, which controls the shear stress contribution to failure, reads

$$\alpha = \frac{f_{tx}\, f_{ty}}{\tau_{u,t}^2} \qquad (4)$$

Here, $f_{tx}$, $f_{ty}$ and $\tau_{u,t}$ are, respectively, the uniaxial tensile strengths in the *x*, *y* directions and the pure shear strength. Note that the material axes are now fixed with respect to a specific frame of reference. Thus, it shall be assumed that all stresses and strains for the elastoplastic algorithm are given in the material reference axes, see also section 2.5.

Eq. (4) can be recast in a matrix form as

$$f_1 = (\tfrac{1}{2}\{\xi\}^T[\mathrm{P}_t]\{\xi\})^{\frac{1}{2}} + \tfrac{1}{2}\{\pi\}^T\{\xi\} \qquad (5)$$

where the projection matrix $[\mathrm{P}_t]$ reads

$$[\mathrm{P}_t] = \begin{bmatrix} \frac{1}{2} & -\frac{1}{2} & 0 & 0 & 0 \\ -\frac{1}{2} & \frac{1}{2} & 0 & 0 & 0 \\ 0 & 0 & 2\alpha & 0 & 0 \\ 0 & 0 & 0 & 0 & 0 \\ 0 & 0 & 0 & 0 & 0 \end{bmatrix} \qquad (6)$$

the projection vector $\{\pi\}$ reads

$$\{\pi\} = \{1 \quad 0 \quad 0 \quad 0 \quad 0\}^T \qquad (7)$$

the reduced stress vector $\{\xi\}$ reads

$$\{\xi\} = \{\sigma\} - \{\eta\} \qquad (8)$$

the stress vector $\{\sigma\}$ reads

$$\{\sigma\} = \{\sigma_x \quad \sigma_y \quad \tau_{xy} \quad \tau_{yz} \quad \tau_{xz}\}^T \qquad (9)$$

and the back stress vector $\{\eta\}$ reads

$$\{\eta\} = \{\sigma_{tx}(\kappa_t) \quad \sigma_{ty}(\kappa_t) \quad 0 \quad 0 \quad 0\}^T \qquad (10)$$

Exponential tensile softening is considered for both equivalent stress-equivalent strain diagrams, with different fracture energies ($G_{fx}$ and $G_{fy}$) for each yield value, which read

$$\bar{\sigma}_{tx} = f_{tx}\exp(-\frac{h f_{tx}}{G_{fx}}\kappa_t)\ ;\ \bar{\sigma}_{ty} = f_{ty}\exp(-\frac{h f_{ty}}{G_{fy}}\kappa_t) \quad (11)$$

where the standard equivalent length $h$ is related to the element size [15].

A non-associated plastic potential $g_1$

$$g_1 = (\tfrac{1}{2}\{\xi\}^T[\mathrm{P}_g]\{\xi\})^{\frac{1}{2}} + \tfrac{1}{2}\{\pi\}^T\{\xi\} \quad (12)$$

is considered, where the projection matrix $[\mathrm{P}_g]$ represents the original Rankine plastic flow, i.e. $\alpha = 1$ in eq. (6).

The inelastic behaviour is described by a strain softening hypothesis given by the maximum principal plastic strain $\dot{\varepsilon}_t^p$ as

$$\dot{\kappa_t} = \dot{\varepsilon}_1^p = \frac{\dot{\varepsilon}_x^p + \dot{\varepsilon}_y^p}{2} + \tfrac{1}{2}\sqrt{(\dot{\varepsilon}_x^p - \dot{\varepsilon}_y^p)^2 + (\dot{\gamma}_{xy}^p)^2} \quad (13)$$

which reduces to the particularly simple expression

$$\dot{\kappa_t} = \dot{\lambda}_t \quad (14)$$

## 2.4 Compression - A Hill Type Criterion

In case of crushing it is physically appealing and it results quite simple to include the contribution of the additional stresses from the shell formulation ($\tau_{yz}$ and $\tau_{xz}$) in the failure criterion.

The simplest yield criterion that features different compressive strengths along the material axes is a rotated centred ellipsoid in the full plane stress space. The expression for such a quadric can be written as

$$f_2 = \frac{\bar{\sigma}_{cy}(\kappa_c)}{\bar{\sigma}_{cx}(\kappa_c)}\sigma_x^2 + \beta\sigma_x\sigma_y + \frac{\bar{\sigma}_{cx}(\kappa_c)}{\bar{\sigma}_{cy}(\kappa_c)}\sigma_y^2 + \gamma(\tau_{xy}^2 + \tau_{yz}^2 + \tau_{xz}^2) - \bar{\sigma}_{cx}(\kappa_c)\,\bar{\sigma}_{cy}(\kappa_c) = 0 \quad (15)$$

where $\bar{\sigma}_{cx}(\kappa_c)$ and $\bar{\sigma}_{cy}(\kappa_c)$ are, respectively, the yield values along the material axes $x$ and $y$. The $\beta$ and $\gamma$ values are additional material parameters that determine the shape of the yield criterion. The parameter $\beta$ controls the coupling between the normal stress values, i.e. rotates the yield criterion around the shear stress axis, and must be obtained from one additional experimental test, e.g. biaxial compression with a unit ratio between principal stresses. The parameter $\gamma$, which controls the shear stresses contributions to failure, can be obtained from

$$\gamma = \frac{f_{cx}\ f_{cy}}{\tau_{u,c}^2} \quad (16)$$

where $f_{cx}$ , $f_{cy}$ and $\tau_{u,c}$ are, respectively, the uniaxial compressive strengths in the $x$, $y$ directions and a fictitious pure shear in compression.

For the purpose of numerical implementation, it is convenient to recast this yield criterion in a matrix form as

$$f_2 = (\tfrac{1}{2}\{\sigma\}^T[\mathrm{P}_c]\{\sigma\})^{\frac{1}{2}} - \bar{\sigma}_c(\kappa_c) \quad (17)$$

where the projection matrix $[\mathrm{P}_c]$ reads

$$[\mathrm{P}_c] = \begin{bmatrix} 2\frac{\bar{\sigma}_{cy}(\kappa_c)}{\bar{\sigma}_{cx}(\kappa_c)} & \beta & 0 & 0 & 0 \\ \beta & 2\frac{\bar{\sigma}_{cx}(\kappa_c)}{\bar{\sigma}_{cy}(\kappa_c)} & 0 & 0 & 0 \\ 0 & 0 & 2\gamma & 0 & 0 \\ 0 & 0 & 0 & 2\gamma & 0 \\ 0 & 0 & 0 & 0 & 2\gamma \end{bmatrix} \quad (18)$$

the yield value $\bar{\sigma}_c$ is given by

$$\bar{\sigma}_c(\kappa_c) = \sqrt{\bar{\sigma}_{cx}(\kappa_c)\,\bar{\sigma}_{cy}(\kappa_c)} \quad (19)$$

and the scalar $\kappa_c$ controls the amount of hardening and softening.

The inelastic law adopted comprehends parabolic hardening followed by parabolic/exponential softening for both equivalent stress-equivalent strain diagrams, with different compressive fracture energies ($G_{fcx}$ and $G_{fcy}$) along the material axes [11]. The problem of mesh objectivity of the analyses with strain softening materials is a well debated issue, at least for tensile behaviour, and the stress-strain diagram must be adjusted according to an equivalent length $h$ to provide an objective energy dissipation [12].

An associated flow rule and a work-like hardening/softening hypothesis are considered. This yields

$$\dot{\kappa_c} = \frac{1}{\bar{\sigma}_c}\{\sigma\}^T\{\dot{\varepsilon}^p\} = \dot{\lambda}_c \quad (20)$$

## 2.5 Orientation of the material axes

For the sake of simplicity, the formulation of the plasticity model was presented based on the assumption that the principal axes of anisotropy coincided with the frame of reference (local or global) for stresses and strains in finite element computations. Since this is not necessarily the case, such non-alignment effects must be taken into account.

Two different approaches can be followed. In the first approach, with each call to the plasticity model, stresses, strains and, finally, consistent tangent stiffness matrices must be rotated into and out of the material frame of reference, respectively, as pre- and post-processing. In the second approach, before the analysis begins, the elastic stiffness matrix [D], the projection matrices $[\mathrm{P}_t]$, $[\mathrm{P}_g]$ and $[\mathrm{P}_c]$, and the projection vectors $\{\pi\}$ and $\{\eta\}$ must be rotated from the material frame of reference into the global frame of reference at each quadrature point, eliminating

the need of all subsequent rotation operations. The drawback of the latter approach is that the matrices then lose their sparse nature, resulting in less clear algorithms. For this reason, the plasticity model is implemented employing the former option.

## 2.6 Behaviour of the Model

The behaviour of the model in uniaxial tension, compression and pure bending along the material axes is given in Figure 5. The values chosen for the material parameters (different tensile strengths, compressive strengths and fracture energies along each material axis) illustrate the fact that completely different behaviour along the two material axes can be reproduced.

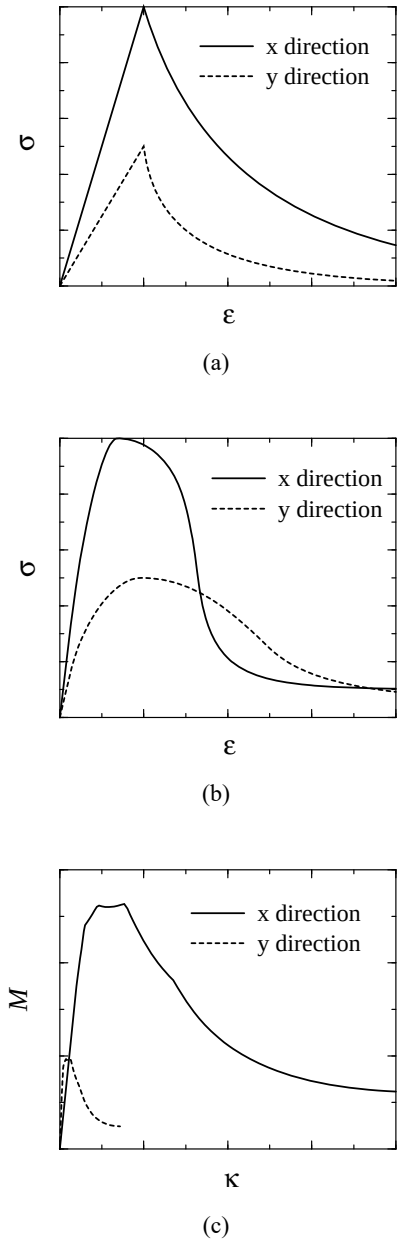


**Figure 5 Possible behaviour of the model along the material axes: (a) uniaxial tension; (b) uniaxial compression; (c) pure bending**

## 2.7 The Concept of Flexural Strength

Two arguments can be used in favour of using bending tests (three-point or four point bending) to obtain the flexural strength of a material. Firstly, the tests are relatively easy and inexpensive to perform and, secondly, if one is dealing with shell analysis it seems natural to directly characterise the bending tests behaviour. Nevertheless, one question that arises in practice is the relation between tensile and flexural strengths.

In the following, we will assume for simplicity that only tensile inelastic behaviour occurs in a structure. For a cross section of a beam or plate in pure bending, see Figure 6, the elementary linear elastic beam theory yields a tensile flexural strength

$$f_{ft} = \frac{6M}{bh^2} \tag{21}$$

where $f_{ft}$ is the flexural tensile strength, $M$ is the bending moment, and $b$, $h$ are the dimensions of the cross section of the beam.

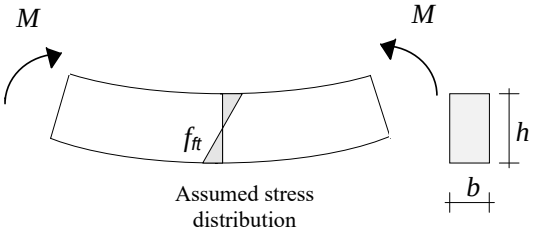


**Figure 6 Beam under pure bending. Linear elastic theory**

But this value is not the real uniaxial tensile strength. If the beam is subjected to increasing load, at a certain stage the tensile strength of the extreme fibre will be reached. The stress in this fibre starts to follow the descending branch, the micro-crack propagates upwards and the neutral axis of the cross section shifts towards the fibres in compression. Although micro-cracking is occurring the bending moment can still be increased until the peak moment is reached. Only at the ultimate stage, a fully developed crack occurs. The internal stress distribution in the cross section through the all process is shown in Figure 7.

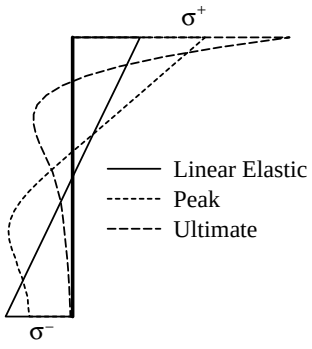


**Figure 7 Normal stress distribution in a cross-section subjected to pure bending**

It is obvious that the influence of the descending branch in the stress-crack width diagram diminishes with increasing height $h$ of the cross-section. As an example, for concrete, the Model Code 90 provides the following expression

$$\frac{f_{ft}}{f_t} = 0.6 + \frac{0.4}{h} \qquad (\geq 1) \qquad (22)$$

where $f_t$ is the uniaxial tensile strength and the height of the cross section $h$ is expressed in meters.

# 3 APPLICATION: MASONRY SHELL PANELS

Masonry is a composite material made of units and mortar. The effective constitutive behaviour of masonry features anisotropy arising from the geometrical arrangement of units and mortar, even if the properties of these constituents are isotropic. The proposed model is, therefore, adopted for the analysis of two masonry rectangular panels for which sufficient experimental data are available, Gazzola *et al* [16]. The masonry panels are simply supported in the four edges and are loaded until failure by a uniformly distributed out-of-plane pressure of increasing magnitude. Two panels with dimensions 5000 × 2800 × 150 mm$^3$ will be analysed: Panel WII and Panel WP1, where the first panel has no in-plane action and the second panel is subjected to a in-plane compressive load of 0.2 N/mm$^2$, see Figure 8. The material axes are defined by the joints directions ($x$- and $y$-axis) and the normal to the plate ($z$-axis)

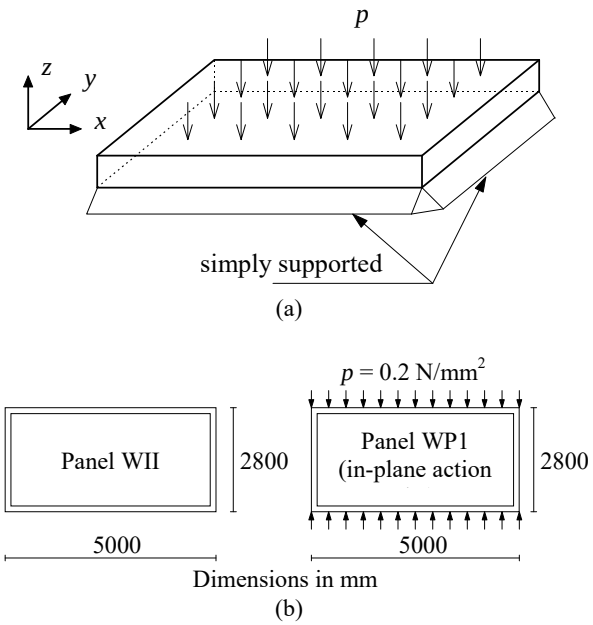


**Figure 8 Masonry shell panels: (a) out-of-plane loading; (b) geometry and in-plane loading**

For the given geometry and loading conditions it was observed in the experiments that only tensile failure occurred. Compressive and mixed tensile-compressive failure are likely to occur in the case of point loads or in the presence of high in-plane stresses. These in-plane stresses arise normally due to the confinement of the supports or the arching action in curved shells, which is not the case here. Therefore, the present example only effectively validates the tensile criterion of the proposed model. In a subsequent publication the tensile and compressive criteria will be evaluated. For the case of plates, the reader is referred to [11] where analyses which activate both regimes of the model are presented.

## 3.1 Inelastic Material Properties

Masonry samples have been tested in four-point bending samples making different orientations with regard to the material axes (0, 15, 45, 75 and 90 degrees) [16]. For each direction five tests have been carried out. Figure 9 shows the results of the tests, represent by the average flexural tensile strength and its standard deviation, and the best fit of the model. It is possible to conclude that the model can reasonably approximate the numerical results.

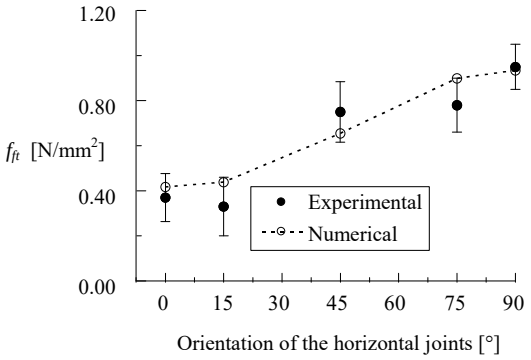


**Figure 9 Comparison between experimental [16] and numerical strengths along different loading directions**

It is noted that eq. (22) was utilised to estimate the uniaxial tensile strength along each material direction ($f_{tx}$ and $f_{ty}$). The fracture energies along each direction ($G_{fx}$ and $G_{fy}$) were then calculated by inverse fitting so that the correct bending moments would be obtained. The inelastic material properties calculated this way are given in Table 1.

**Table 1 Inelastic material properties**

| $f_{tx}$ | $f_{ty}$ | α | $G_{fx}$ | $G_{fy}$ |
|---|---|---|---|---|
| 0.95 N/mm$^2$ | 0.35 N/mm$^2$ | 0.40 | 0.90 N.mm/mm$^2$ | 0.06 N.mm/mm$^2$ |

## 3.2 Results

Figure 10 shows the load-centre displacement diagram obtained in the numerical analysis. This gives a good impression about the numerical implementation because it is possible to trace the response of the structure through initial cracking, failure load and post-failure behaviour. The comparison with the experimental failure loads is shown in Figure 10 and Table 2. Good agreement is found because the difference between predicted and observed results is smaller that 10 %. Noteworthy is the fact that a

small confinement (pre-compression of 0.2 N/mm$^2$) gives an increase of strength of 30 %.

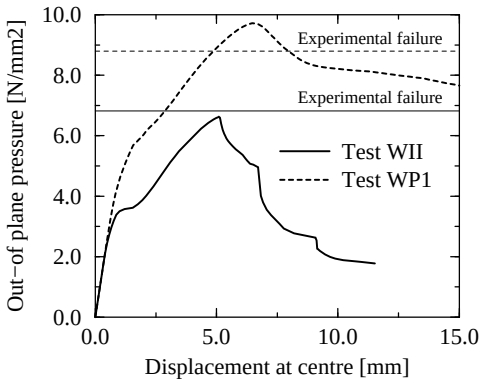


**Figure 10 Numerical load-displacement diagrams and experimental failure loads [16]**

**Table 2 Numerical vs. experimental failure loads**

| Panel | WII | WP1 |
|---|---|---|
| $p_{exp}$ [N/mm$^2$]$^\dagger$ | 6.82 | 8.80 |
| $p_{num}$ [N/mm$^2$] | 6.59 | 9.72 |
| Num. / Exp. | **0.97** | **1.10** |

$^\dagger$ Experimental results are the average of three tests

The results in terms of (incremental) deformed meshes at ultimate stage are represented in Figure 11. The cracking contours are illustrated in Figure 12. Cracking is represented by the equivalent plastic strain. The figure shows that slightly different failure modes are obtained for both panels. The yield-line type of results, typical of shell analysis, shows that the yield-line parallel to the panel side is closer to the sides of the panel for WII and is closer to the centre of the panel for WP1.

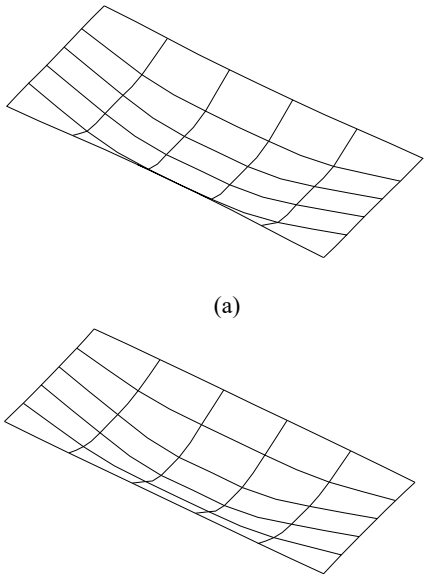

(a)

(b)

**Figure 11 Incremental deformed mesh: (a) WII at ultimate stage; (b) WP1 at ultimate stage**

## 4 CONCLUSIONS

An elastoplastic model for the analysis of anisotropic plates and shells has been presented. The model is especially suited for materials which feature a large difference in magnitude between uniaxial tensile and compressive strengths.

Application of the model to the analysis of masonry shell panels demonstrated the good performance of the model and the robustness of the numerical implementation.

## 5 ACKNOWLEDGEMENTS

The calculations have been carried out with the DIANA finite element code of TNO Building and Construction Research. This research has been supported financially by the Netherlands Technology Foundation (STW) under grant DCT 33.3052. The author gratefully acknowledges the support of the project leader Dr.ir. Jan G. Rots from TNO Building and Construction Research, The Netherlands

## 6 REFERENCES

[1] R. Hill, *A theory of the yielding and plastic flow of anisotropic metals*, Proc. Roy. Soc., (London) A, 193, 281-288, 1948.

[2] O. Hoffman, *The brittle strength of orthotropic materials*, J. Composite Mat., 1, 200-206, 1967.

[3] S.W. Tsai and E.M. Wu, *A general theory of strength of anisotropic materials*, J. Composite Mat., 5, 58-80, 1971.

[4] R. de Borst and P.H. Feenstra, *Studies in anisotropic plasticity with reference to the Hill criterion*, Int. J. Numer. Methods Engrg., 29, 315-336, 1990.

[5] J.C.J. Schellekens and R. de Borst, *The use of the Hoffman yield criterion in finite element analysis of anisotropic composites*, Comp. Struct., 37(6), 1087-1096, 1990.

[6] J.F. Besseling, *A theory of elastic, plastic and creep deformations of an initially isotropic material showing anisotropic strain-hardening, creep recovery and secondary creep*, J. Appl. Mech., 22, 529-536, 1958.

[7] D.R.J. Owen and J.A. Figueiras, Elasto-plastic analysis of anisotropic plates and shells by the semiloof element, Int. J. Numer. Methods Engrg., 19, 521-539, 1983.

[8] C.C. Swan and A.S. Cakmak, *A hardening orthotropic plasticity model for non-frictional composites: Rate formulation and integration algorithm*, Int. J. Numer. Methods Engrg., 37, 839-860, 1994.

[9] X. Li, P.G. Duxbury and P. Lyons, *Considerations for the application and numerical implementation of strain hardening with the Hoffman yield criterion*, Comp. Struct., 52(4), 633-644, 1994.

[10] P.B. Lourenço, *Computational strategies for masonry structures*, Dissertation, Delft University of Technology, Delft, The Netherlands, 1996.

[11] P.B. Lourenço, R. de Borst and J.G. Rots, *A plane stress softening plasticity model for orthotropic materials*, Int. J. Numer. Methods Engrg., 1997 (accepted for publication).
[12] P.H. Feenstra and R. de Borst, *A composite plasticity model for concrete*, Int. J. Solids Structures, 33(5), 707-730, 1996.
[13] S. Ahmad, B.M. Irons and O.C. Zienkiewicz, *Analysis of thick and thin shell structures by curved finite elements*, Int. J. Numer. Methods Engrg., 2, 419-451, 1970.
[14] P.H. Feenstra and R. de Borst, *A plasticity model and algorithm for mode-I cracking in concrete*, Int. J. Numer. Methods Engrg., 38, 2509-2529, 1995.
[15] Z.P. Bazant and B.H. Oh, *Crack band theory for fracture of concrete*, Materials and Structures, RILEM, 93(16), 155-177, 1983.
[16] E.A. Gazzola, R.G. Drysdale and A.S. Essawy, *Bending of concrete masonry walls at different angles to the bed joints*, Proc. of the Third North American Masonry Conference, Arlington, Texas, Paper 27, 1985.

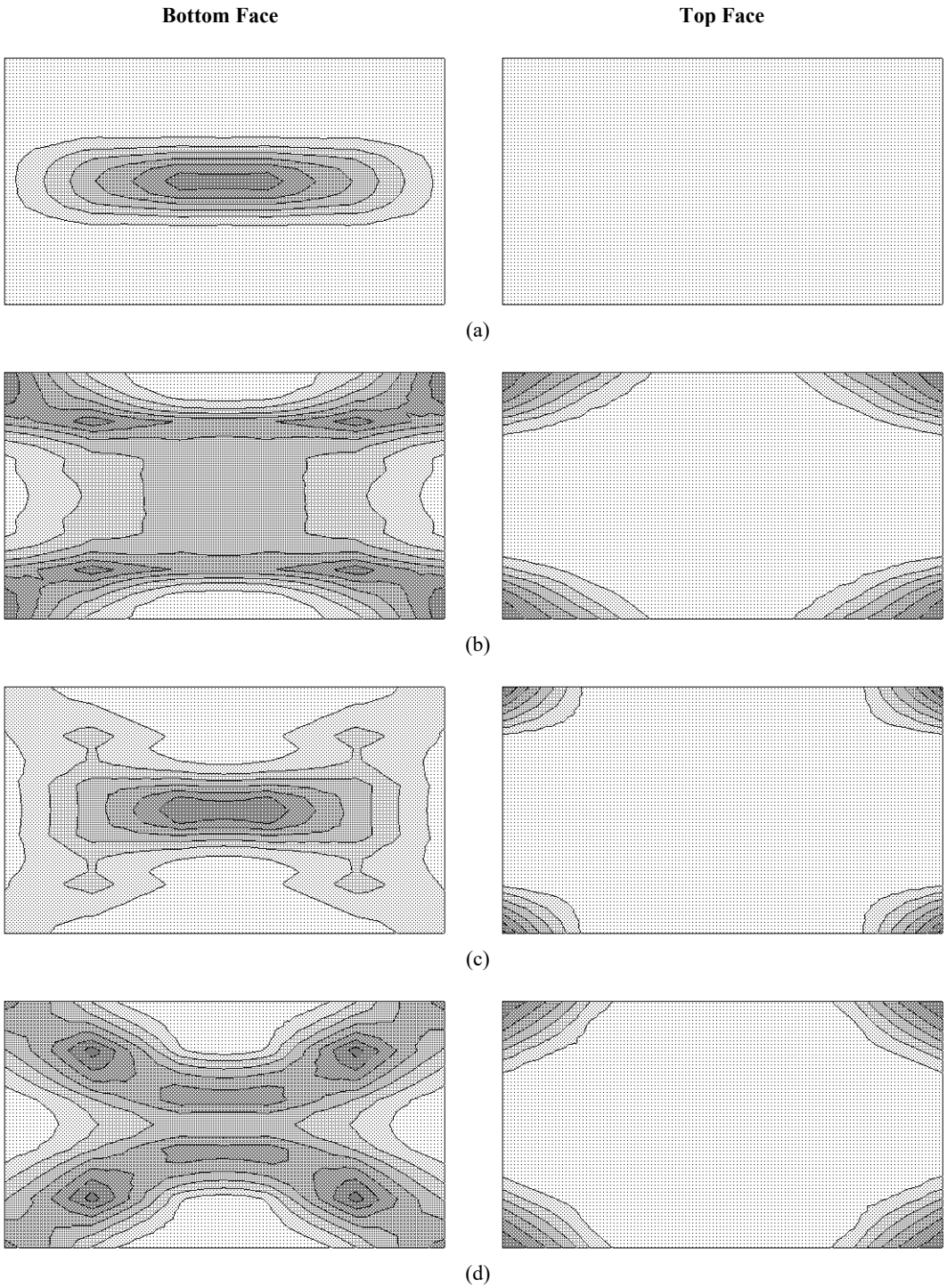


**Figure 12 Cracking: (a) WII at peak; (b) WII at ultimate stage; (c) WP1 at peak; (d) WP1 at ultimate stage**